Magnetic Navigation Using Online Calibration Filter Analysis

THESIS

Jonnathan D. Bonifaz, B.S.E.E.

AFIT-ENG-MS-22-M-010

DEPARTMENT OF THE AIR FORCE
AIR UNIVERSITY

AIR FORCE INSTITUTE OF TECHNOLOGY

Wright-Patterson Air Force Base, Ohio

AFIT-ENG-MS-22-M-010

Magnetic Navigation Using Online Calibration Filter Analysis

THESIS

Presented to the Faculty

Department of Electrical and Computer Engineering

Graduate School of Engineering and Management

Air Force Institute of Technology

Air University

Air Education and Training Command

in Partial Fulfillment of the Requirements for the

Degree of Master of Science in Electrical Engineering

Jonnathan D. Bonifaz, B.S.E.E., B.S.E.E.

March 24, 2022

AFIT-ENG-MS-22-M-010

Magnetic Navigation Using Online Calibration Filter Analysis

THESIS

Jonnathan D. Bonifaz, B.S.E.E., B.S.E.E.

Committee Membership:

Maj. Joseph A Curro, Ph.D
Chair

Robert C Leishman, Ph.D
Member

Clark N Taylor, Ph.D
Member

Abstract

Magnetic navigation using the Earth's magnetic anomaly field has proven to be a promising alternative that can provide coverage for a navigation system. This research demonstrates a magnetic navigation system using an extended Kalman filter (EKF) to aid an aircraft's inertial navigation system (INS). Traditional magnetic anomaly navigation uses a "static calibration method," which takes post-processed data to calibrate, obtaining the Tolles-Lawson coefficients needed for magnetic anomaly navigation filter compensation. These coefficients are constant and may cause drifts in the navigation filter if not re-calibrated. The online calibration method continuously updates the Tolles-Lawson coefficients as a state of the filter, reducing the need for calibration flights. This research uses F-16 data to demonstrate the effectiveness of this method.

Table of Contents

Page

List of Figures

List of Tables

Magnetic Navigation Using Online Calibration Filter Analysis

I. Introduction

1.1 Problem Background

The Global Positioning System (GPS) is the primary navigation system used by various platforms in the Department of Defence (DOD) or Air Force. It is a system that is available worldwide and is passive for the user. However, GPS is highly susceptible to jamming or spoofing. The navigation community has stressed the need for alternative navigation techniques. A technique that has had high interest is magnetic anomaly navigation. It has shown promise, and it is passive and not so easily jammed or spoofed like GPS.

1.1.1 Magnetic Anomaly Navigation

Magnetic anomaly navigation uses scalar intensity measurements with vector measurements of the Earth's magnetic field. This alternate form of navigation uses a reference map of the magnetic anomaly of the Earth to estimate the position and aid inertial measurements. The increase of interest in this type of navigation is rising because Earth's magnetic anomaly field is available worldwide and magnetic field sensors are entirely passive. Previous research in magnetic anomaly navigation has shown great effectiveness in ideal conditions [1]. Traditionally magnetic anomaly navigation has used a static calibration. This calibration is done with post-processed data for calibration. Then these parameters are then used in the next flight for the navigation filter to compensate the aircraft disturbance field and estimate the measurements.

Due to various conditions and operational objectives, the platform may change its configuration, or other conditions may cause calibration perimeters to lose accuracy. This calibration drift has given researchers interest in a calibration type that will continuously update the calibration parameters as the platform operates.

1.2 Research Objectives

There are two areas explored in this thesis. The first is to implement in NavToolKit both static and online calibration magnetic anomaly navigation filters. The second is to test the online calibration magnetic anomaly filter with data recorded from an F-16 aircraft. Both static and online calibration filters will be compared. The main focus is to analyze the online calibration filter performance. The filter's performance shows the benefit of using online calibration over static calibration for aircraft as the use of magnetic navigation in DOD or Air Force operations. Online is more operational friendly because it reduces the need for calibration flights. In real-world operations, the aircraft will not fly a calibration flight, then use that data to get the calibration coefficient, fly the mission using the calibrations coefficients, and fly calibration flights before each mission. A more realistic operational scenario would be to fly a single calibration flight to initialize the online calibration. Then have the navigation filter continuously update these calibration coefficients. Also, if GPS is available, the calibration can be updated more accurately. Online calibration lessens the need for calibration flights.

1.3 Document Overview

This thesis is organized into five chapters. Chapter I introduces magnetic navigation and the need for online calibration. Chapter II provides the background needed to perform magnetic anomaly navigation using Tolles-Lawson compensation.

Chapter III details the methodology used to conduct this research. This chapter also provides the method used to analyze F-16 magnetic field data. Chapter IV discusses the results of the simulations and analysis. Finally, Chapter V contains with a summary of the results and future work needed to improve online calibration.

II. Background and Literature Review

This chapter provides the background of aeromagnetic navigation and an overview of related work. section 2.1 details the components that make up the Earth's magnetic field. section 2.2 provides an overview of Aeromagnetic navigation. Also, the concepts required for obtaining the position estimate are detailed. Section 2.3 covers the extended Kalman Filter (EKF), and Section 2.4 the 15 state Pinson, inertial navigation system (INS) error model. Section 2.6 highlights the plug-and-play framework of NavToolKit.

2.1 Earth Magnetic Field Components

The Earth's magnetic field components consist of four sources. Three of the four primary measurable sources are the core, anomaly, and space weather effects. Aircraft effect is the fourth source and will be discussed in more detail in section 2.2.2.1

2.1.1 Core Field

The component that contributes the most to the Earth's magnetic field is the core field. This field of electromagnetic currents is generated deep within the Earth's inner core [3]. The Earth's inner core is a liquid core that contains conductive molten iron. The average magnitude of the core field is about 50,000 nT, and it varies by approximately ±20,000 nT based on global location[4]. This core field can be exemplified when looking at a compass pointing North, it acts as a dipole along the Earth's axis of rotation. The core field has variations that change slowly, and the changes are not very significant every year. The core field variations are accounted for and remodeled every five years [5]. Systems like the World Magnetic Model (WMM) model the Core field well . The WMM is a joint product of the United States

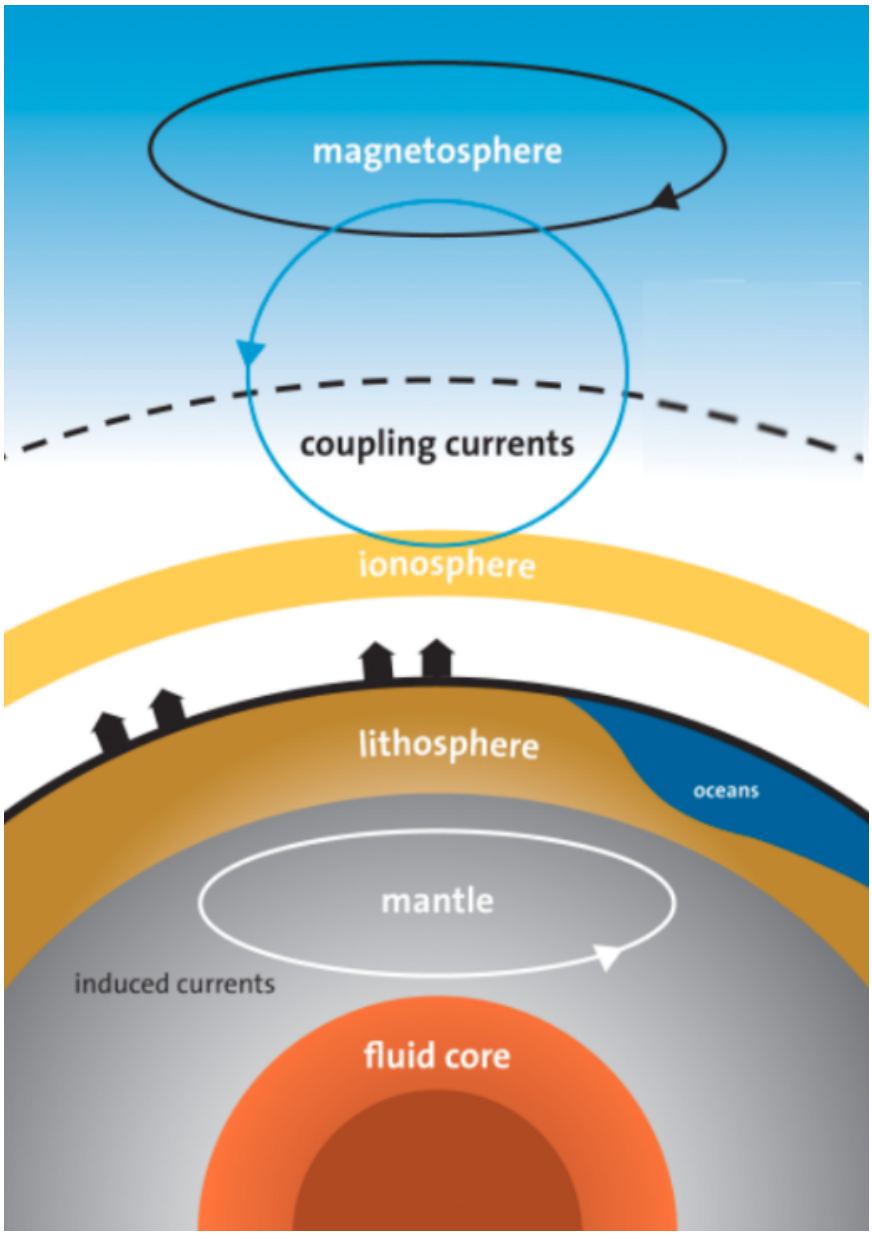

Figure 1: Earth's magnetic field sources [2]

National Geospatial-Intelligence Agency (NGA) and the United Kingdom's Defence Geographic Centre (DGC). The core field is a low-frequency signal containing spatial wavelengths in thousands of kilometers. Because of the spatial variation of the core field, a magnetic navigation system can not use it for navigation. Figure 2 shows the lack of spatial variation in the Core field[5].

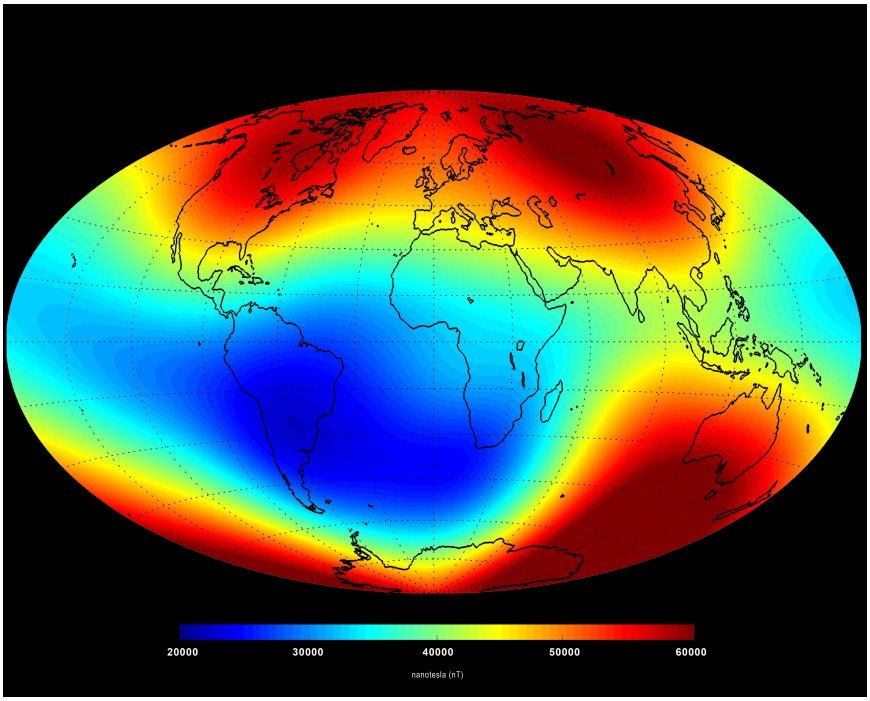

Figure 2: Earth's core field at Earth's surface [6]

2.1.2 Anomaly Field

The anomaly field is calculated form the Earth's Crust field and Earth's core field. Earth's crustal field, or lithosphere field, is caused by the permanent or induced magnetization of rocks in the Earth's crust. The Earth's core and crust fields are used in the calculation to measure the anomaly field. Magnetic navigation uses this anomaly field measurement. The Earth's crust comprises of different materials that are magnetically susceptible. These materials can have magnetic fields induced by the Earth's core field. The Earth's crust field ranges in the hundreds of nano-Tesla. Compared to the Earth's core field, the Earth's crustal field is significantly smaller.

The Magnetic anomaly field is the scalar deviation from a reference field. The reference field is the core Earth field, and the anomalies come from the Earth's crustal field[1]. This anomaly field has a frequency content that is significantly higher than the core field. Magnetic navigation uses high-frequency content maps of the anomaly

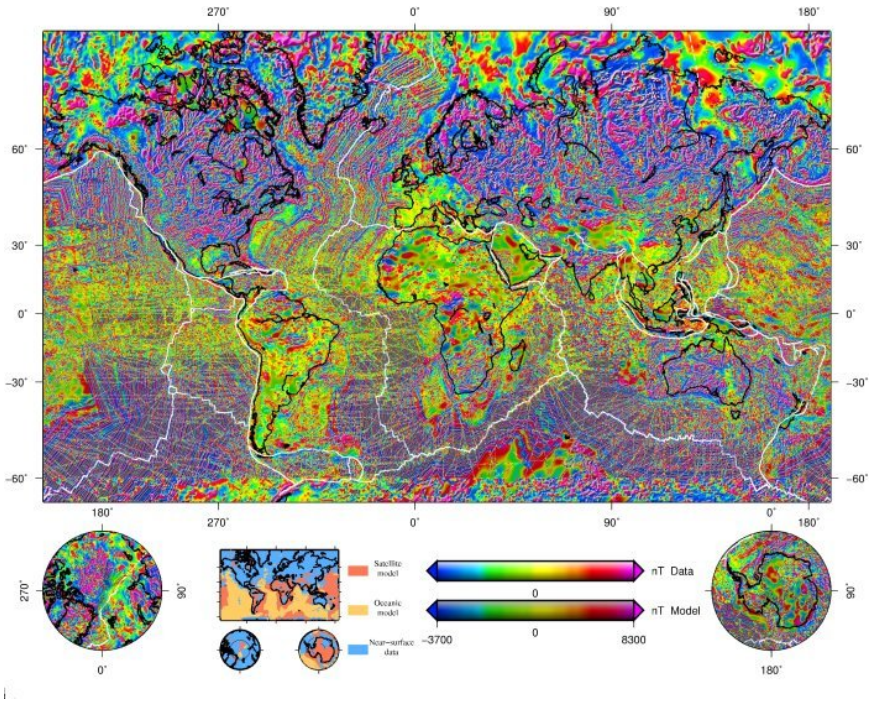

Figure 3: World Digital Magnetic Anomaly Map [7]

field as a reference.

2.1.2.1 Anomaly Definition

The following is a derivation to define the anomaly field. The total magnetic field (B_{total}) is a vector summation of the Earth's core field (B_{core}) and the magnetic anomaly field ($B_{anomaly}$), as in eq. (1).

$$B_{total} = B_{core} + B_{anomaly} \tag{1}$$

An approximation of the magnetic anomaly's magnitude is the scalar subtraction of the core field from the core field, shown in eq. (1).

$$||B_{anomaly}|| \approxeq ||B_{total}|| - ||B_{core}|| \tag{2}$$

The scalar anomaly approximation represents the projection of the magnetic

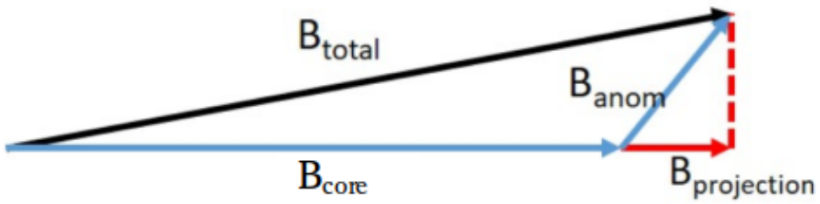

Figure 4: Projection of magnetic anomaly onto the core Earth field

anomaly along the reference field direction, in this case, the Earth's core field. This approximation is only valid when $||B_{core}|| >> ||B_{anomaly}||$[1]. Figure 4 illustrates this vector projection, the length of the anomaly vector is exaggerated for reader visibility, as the core field vector is much greater that the anomaly vector. [4].

2.1.3 Space Weather Effects

The space weather effects are time-varying components from space interacting with the Earth's magnetic field components. This time-varying field corrupts magnetic measurements, and its effects are unpredictable. The temporal variations originate in the ionosphere, and magnetosphere, see Figure 1. Contributions include coupling of the magnetosphere sources and the ionosphere sources, and others [8]. The ionosphere is ionized by solar radiation, creating an electrically conducting plasma where electric currents flow. As the electrically conducting plasma moves relative to the core Earth magnetic field, electric currents develop, creating magnetic fields. The magnetic field induced from differential solar heating is called the Sq, or "solar quiet" variations. The "Solar-Quiet (Sq) currents" produce magnetic fields of their own. Another primary ionospheric current system is the auroral currents. The transient currents influenced by the surface activity of the Sun cause auroral currents[8].

The space surrounding the Earth in which charged particles from the Sun interact with the Earth's magnetic field is called the Earth's magnetosphere. The currents of the magnetosphere are driven primarily by the solar wind coming from the Sun. These

interactions can cause currents, which create their magnetic fields. These currents primarily drive the magnetosphere field. Ring currents are electric currents carried by charged particles trapped in a planet's magnetosphere. The magnetopause current is the abrupt boundary between a magnetosphere and the surrounding plasma. These currents and more can be seen on Figure 5 [9].The daily cycle for these variations are on the order of 10s of nano-Teslas [10].

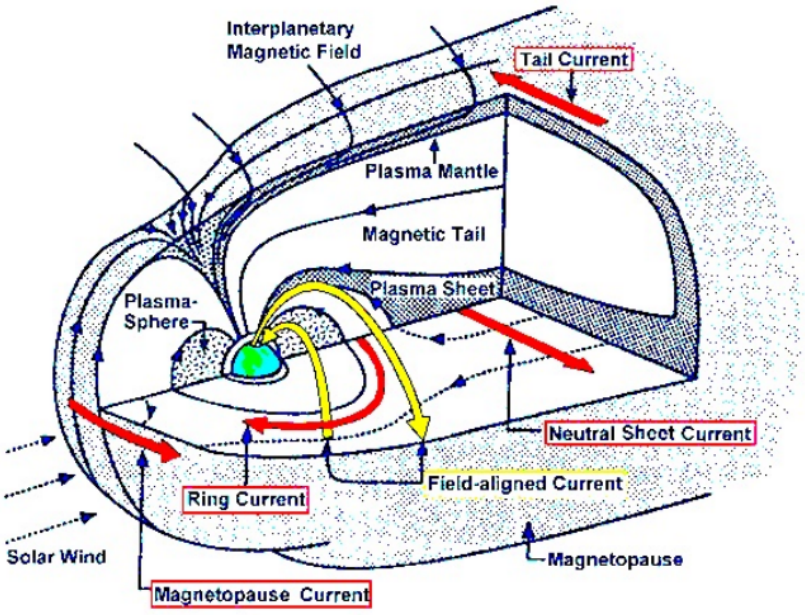

Figure 5: Magnetospheric Currents [9]

2.2 Aeromagnetic Navigation

Aeromagnetic navigation using magnetic anomaly fields can overcome drawbacks from other types of navigation. Magnetic navigation allows for navigation in deserts, oceans, and other types of areas. The anomaly field availability allows magnetic navigation to overcome the drawbacks of weather, visibility, and other features within the area. Another advantage is that magnetic fields are much less susceptible to jamming or spoofing than electromagnetic signals. Canciani's work [1] presented a navigation filter that utilizes scalar magnetic intensity measurements of the Earth's anomaly field to aid an aircraft's INS. A marginalized particle filter compares anomaly field measurements to a map of anomaly field values. They were able to demonstrate the navigation accuracy of the system, obtaining a DRMS error of 13 meters with data in ideal conditions [1].

2.2.1 Measurements and Sensors

Magnetic anomaly navigation requires two types of magnetic measurements: scalar and vector. The B_{total} is the measurement from the scalar magnetometer. The vector magnetometer measurements are only used in calibration to compensate for aircraft effects. Magnetic navigation sensors are generally low in size, weight, and power (swp). These sensors can be carried or positioned onboard an aircraft and are passive devices.

2.2.1.1 Scalar Measurements and Sensors

The scalar magnetometer sensor measurement captures a surrounding magnetic field's total intensity or magnitude. Modern scalar magnetometers have accuracies of the order of 1 nano-Tesla and sensitivities on pico-Teslas [5]. A scalar magnetic intensity measurement would be a constant at a given point in time and space, inde-

pendent of the orientation of the measurement. Scalar magnetometer measurements are the primary reference when using scalar magnetic anomaly maps for navigation and are used to obtain the navigation signal. When scalar magnetometer sensors are on aircraft, the scalar measurements include a corrupting magnetic field beyond the Earth's anomaly field, which will be further discussed in Section 2.2.2.

2.2.1.2 Vector Measurements and Sensors

Vector magnetometer sensors measurements capture the individual components of the surrounding magnetic field, where B_x, B_y, B_z are the individual components. The orientation of these components is along the axes of the vector measurement sensor. Both the magnitude and the direction information are measured with these sensors. Vector magnetometers have worse performance at low frequencies, which magnetic navigation uses [1]. Aircraft magnetic compensation uses vector magnetometer measurements for some forms of compensation. The vector measurements allow for observing the magnetic field changes based on the aircraft's orientation. The vector measurements include the same corrupting magnetic fields as the scalar measurements. The aircraft magnetic compensation concept is further described in Section 2.2.3.

2.2.2 In flight measurement

Aeromagnetic navigation uses the Earth's magnetic anomaly field as the navigational signal. The anomaly field cannot be measured directly in flight, however it can be isolated from the scalar magnetic intensity measurements. The scalar magnetic measurement measures the total magnetic intensity of the surrounding magnetic field. This total magnetic intensity consists of four components in a flight environment.

1. Earth's Core Field

2. Earth's Anomaly Field

3. Space Weather Effects

4. Aircraft Disturbance Field

Non-anomaly field components can be considered measurement errors or corrupting sources [1]. There are methods for removing the corrupting sources from the total magnetic intensity. The most accessible corrupting source to remove is the Earth's core field. The core field, as previously discussed, has an average magnitude of about 50,000 nT. This magnitude is much greater than any of the other corrupting sources. The core field changes slowly over the aircraft's position in the WMM models. The core field can be known even if the position is not known precisely, allowing the removal of the core field from the total intensity measurements.

2.2.2.1 Aircraft Disturbance Field

The aircraft disturbance field is the most challenging component to remove from the total intensity measurement. The aircraft's generated magnetic fields make up the aircraft disturbance field. These fields are caused primarily by magnetically sensitive

Figure 6: Tail mounted stinger on survey aircraft. [11]

materials of the aircraft and their orientation with, and flow through, the Earth's core field [10]. Additionally, aircraft systems and electronics can cause disturbances depending on the component's size, power, function, and relative location to the magnetometers.

Three types of disturbance sources are caused by magnetically sensitive aircraft materials:

1. Permanent magnetization
2. Induced magnetization
3. Eddy currents

Magnetic components of the aircraft cause the aircraft's permanent field. A permanent magnet, for example, creates a field on board the aircraft, which impairs the magnetometer's ability to accurately measure the Earth's magnetic field. This field is a relatively constant magnitude to the aircraft, but its direction changes with attitude [10]. Magnetically permeable materials of an aircraft flying in an external magnetic field, the Earth's magnetic field, causes the induced aircraft field. The aircraft's orientation within the Earth's magnetic field significantly contributes to the magnitude and direction of the aircraft's induced magnetic field [1].The aircraft engine, often magnetically susceptible, will typically create a large, induced field. Eddy currents are electrical currents running through conductive materials on the aircraft. According to Faraday's law of induction, these electrical currents are caused by conductive material moving within an external magnetic field. The Eddy currents create their corrupting magnetic field following the Bio-Savart law [1], which describes the magnetic field generated by an electric field.

The preferred method for reducing the aircraft disturbance field is to place magnetometers as far away from disturbance-causing sources as possible. Geo-survey

aircraft typically use a "stinge" to place the magnetometers far away from the aircraft engines, their primary source of the induced disturbance. Figure 6 shows a tail-mounted stinger on a geo-survey aircraft. Magnetometer placement must still be studied and considered, as it is by far the most effective means of reducing the aircraft disturbance field. Aircraft magnetic compensation systems can estimate and remove the aircraft's magnetic fields based on the orientation of the aircraft within the Earth's magnetic field [1]. Additionally, compensation systems can incorporate other known and observable corrupting sources (i.e., aircraft systems and electronics) into the compensation estimation methods [12]. Section 2.2.3 introduces traditional aircraft compensation methods used in previous research on magnetic navigation.

2.2.3 Traditional Calibration and Tolles-Lawson

Tolles lawson's compensation model divides the aircraft's disturbance field into three parts: the permanent magnetic field, induced magnetic field, and eddy current magnetic field. Eighteen coefficients represent the compensation parameters, a mathematical model for predicting the aircraft disturbance field During the flight,

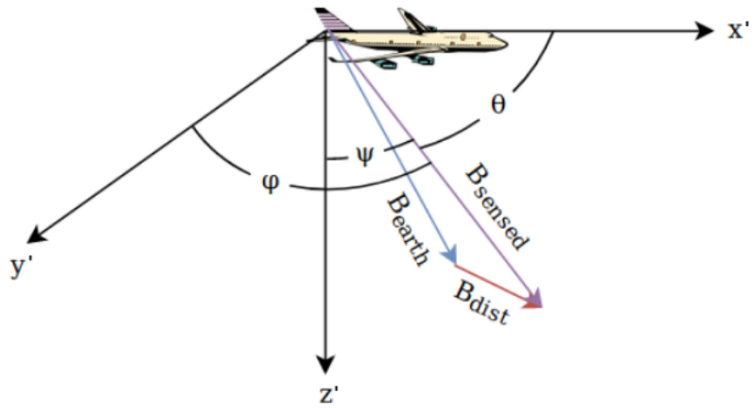

Figure 7: Aircraft reference frame used during aeromagnetic compensation [13]

the onboard scalar magnetometer reads Earth's magnetic field intensity given by:

$$B_{sensed}(\boldsymbol{x}, \boldsymbol{\theta}) = B_E(x) + B_{dist}(\boldsymbol{x}, \boldsymbol{\theta}, \epsilon) \tag{3}$$

where,

$\boldsymbol{x} = \begin{bmatrix} x & y & z \end{bmatrix}^T$ denotes the spatial positioning of the magnetometer on Earth with repect to the aircraft,

$\boldsymbol{\theta} = \begin{bmatrix} \theta & \phi & \psi \end{bmatrix}^T$ denote the aircraft's orientation relative to the geomagnetic field vector

Each term in $\boldsymbol{\theta}$ denotes the angle between the geomagnetic vector and one of the aircraft's primary axes. Since the scalar magnetic values measure the intensity and not direction, we know that the platform effects are often highly correlated with the aircraft's orientation with respect to the geomagnetic vector.

In (3) the B_{sensed} is the scalar magnetometers measurements of the B_E and B_{dist}. This measurement output is the primary reference when using scalar magnetic anomaly maps for navigation. B_E is the Earth's magnetic field that the WMM can reference. B_{dist} consists of all the corrupting sources, and the most significant component comes from aircraft effects. However, this term encompasses all nuisance sources of magnetic disturbances.

The magnetic disturbances are compensated with the Tolles-Lawson compensation model [14]. The Tolles-Lawson equations, given in their modern form in [15], assert that the disturbance field can be modeled by:

$$B_{dist} = B_{perm} + B_{ind} + B_{eddy} \tag{4}$$

B_{perm} is the portion of the disturbance field created by objects in the aircraft with

permanent magnetization. B_{ind} is from magnetically susceptible materials, which produce an induced magnetic field when placed inside the Earth's core field. B_{eddy} models the effects of eddy currents; undesired currents created in the bulk of a conductor similar in nature to induced currents. Eighteen coefficients are estimated to predict the B_{dist} field and include three permanent, six induced, and nine eddy current magnetization coefficients [14].

The compensation coefficients can be obtained by the least squares solution from eq. (5) assuming $\boldsymbol{A}$ is the matrix of the direction cosines, y is the aircraft disturbance, and x represents the 18 Tolles-Lawson coefficients to be fitter by the least squares solution.

$$y = \boldsymbol{A}_{1x18}\boldsymbol{x}_{TL18x1} \tag{5}$$

The $\boldsymbol{A}$ matrix is represented by:

$$\boldsymbol{A} = \begin{bmatrix} \cos\theta \\ \cos\psi \\ \cos\phi \\ B_t \cos\theta^2 \\ B_t \cos\theta \cos\psi \\ B_t \cos\theta \cos\phi \\ B_t \cos\psi^2 \\ B_t \cos\psi \cos\psi \\ B_t \cos\phi^2 \\ B_t \cos\theta \cos\dot{\theta} \\ B_t \cos\theta \cos\dot{\psi} \\ B_t \cos\theta \cos\dot{\phi} \\ B_t \cos\psi \cos\dot{\theta} \\ B_t \cos\psi \cos\dot{\psi} \\ B_t \cos\psi \cos\dot{\phi} \\ B_t \cos\phi \cos\dot{\theta} \\ B_t \cos\phi \cos\dot{\psi} \\ B_t \cos\phi \cos\dot{\phi} \end{bmatrix}_{18x1} \tag{6}$$

where,

B_x, B_y, B_z are the magnetic flux along the i-th aircraft axis, as in fig. 7.

$\cos\theta = B_x/B_t$ is the X direction cosine term

$\cos\psi = B_y/B_t$ is the Y direction cosine term

$\cos\phi = B_z/B_t$ is the Z direction cosine term

B_t is the raw scalar magnetometer measurement

The different components of Equation 4 are defined as [16] :

$$
\begin{aligned}
B_{perm} &= a_1 \cos\theta + a_2 \cos\phi + a_3 \cos\psi \\
B_{ind} &= B_t(a_4 \cos^2\theta + a_5 \cos\theta\cos\phi + a_6 \cos\theta\cos\psi + a_7 \cos^2\phi + a_8 \cos\phi\cos\psi + a_9 \cos^2\psi) \\
B_{eddy} &= B_t(a_{10} \cos\theta(\cos\theta)' + a_{11} \cos\theta(\cos\phi)' + a_{12} \cos\theta(\cos\psi)' \\
&\quad + a_{13} \cos\phi(\cos\theta)' + a_{14} \cos\phi(\cos\phi)' + a_{15} \cos\phi(\cos\psi)' \\
&\quad + a_{16} \cos\psi(\cos\theta)' + a_{17} \cos\psi(\cos\phi)' + a_{18} \cos\psi(\cos\psi)')
\end{aligned}
\tag{7}
$$

The use of the 3-axis vector magnetometer is essential. The vector magnetometer sensor measures the magnetic direction and orientation of the aircraft within the earth field. A calibration flight to collect the data for a Tolles-Lawson calibration is used to compensate for platform-induced effects. During a calibration flight, the aircraft flies in an area where the geomagnetic field varies as little as possible and away from other sources of magnetic disturbance to isolate the aircraft's effect on the magnetometer. The aircraft flies in a tight pattern to ensure that the area's magnetic gradient is flat or linear over the calibration flight. A space where the geomagnetic field has a low gradient indicates a flat, constant field, and flying through that field should ideally not cause any variation in the scalar magnetometer.

Calibration flights typically include flying in four orthogonal directions and performing small-angle banking maneuvers along with each heading, normally 5° to 10° [15]. The maneuvers consist of actuating the ailerons, elevator, and rudder to induce roll, pitch, and yaw maneuvers, see fig. 8 for a example. These maneuvers are critical for seeing the aircraft's orientation with respect to the geomagnetic vector. The

variation in the measurements from aircraft attitude changes is used to determine the calibration coefficients, which can estimate the aircraft disturbance field for the rest of the flight or following flights.

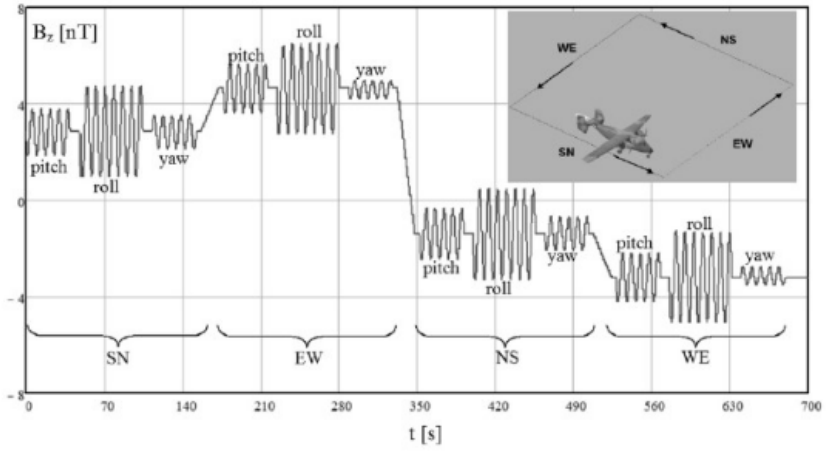

Figure 8: Fixed wing aircraft with stinger seen extending beyond the rudder. [10]

2.3 Extanded Kalman Filter

The extended Kalman filter (EKF) is the traditional estimation method used for non-linear dynamics or non-linear measurement models applications. While it may not be the best solution for magnetic navigation it is a simple and computationally inexpensive method to apply to a navigation system that utilizes magnetic measurements. This section provides the basic equations needed to implement an EKF following [17], referenced for the full derivation. System state dynamics and measurement models are governed by non-linear functions f and h, respectively. The non-linear system is expressed as

$$\boldsymbol{x}_k = f(\boldsymbol{x}_{k-1}, \boldsymbol{u}_k) + \boldsymbol{w}_k \tag{8}$$

$$\boldsymbol{z}_k = h(\boldsymbol{x}_k) + \boldsymbol{v}_k \tag{9}$$

where

$\boldsymbol{x}_k$ is the state vector at discrete time step k

$\boldsymbol{x}_{k-1}$ is the state vector at the previous time step

$\boldsymbol{u}_k$ is the input vector at time k

$\boldsymbol{w}_k$ is the additive white Gaussian noise (AWGN) vector of the state dynamics model, with covariance matrix $\boldsymbol{Q}$

$\boldsymbol{z}_k$ is the measurement vector at time k

$\boldsymbol{v}_k$ is the AWGN vector of the measurement model, with covariance matrix $\boldsymbol{R}$

Like the Kalman filter, the EKF implements propagation and measurement update steps to estimate the system's states. The state estimates are normally distributed

and are defined by an estimated mean vector ($\hat{\boldsymbol{x}}$) and covariance matrix ($\boldsymbol{P}$). Measurement updates are denoted with a minus sign ($-$) before and with a plus sign ($+$) after a measurement update. Each time step is denoted by a subscript k, where $k-1$ would mean the previous time step.

2.3.1 Linearization and Jacobian Matrices

If the functions f and h of the system state are non-linear. They will have to be linearized to form their respective Jacobian matrices $\mathbf{F}$ and $\mathbf{H}$. The linearization is performed by the first order Taylor series expansion, and the Jacobians will be defined as:

$$\boldsymbol{F_k} \triangleq \left.\frac{\delta f(x,u)}{\delta x}\right|_{x=\hat{x}_k^+} \tag{10}$$

$$\boldsymbol{H_k} \triangleq \left.\frac{\delta h(x)}{\delta x}\right|_{x=\hat{x}_k^-} \tag{11}$$

2.3.2 State Propagation

The propagation step propagates the state mean vector and covariance matrix forward in time. Propagation is performed with

$$\hat{x}_k^- = f(x_{k-1}^+, u_k) \tag{12}$$

$$P_k^- = \Phi_{k-1} P_{k-1}^+ \Phi_{k-1}^T + Q_d \tag{13}$$

where,

Φ is the matrix exponential of the state dynamics Jacobian matrix, F

Q_d is a discretized version of the dynamics model noise covariace matrix, Q [18].

2.3.3 Measurement Update

The next step is to update the states of the EKF with the measurement. The measurement update is performed with

$$\hat{x}_k^+ = \hat{x}_k^- + K_k[z_k - h(\hat{x}_k^-, k)] \tag{14}$$

$$P_k^+ = (I - K_k H_k) P_k^- \tag{15}$$

where,

I is the identity matrix

K is the Kalman Gain term defined by

$$K_k = P_k^- H^T [H P_k^- H^T + R]^{-1} \tag{16}$$

2.4 15 State Pinson INS Error Model

A set of 15 state blocks that model the errors of an INS of the complex and non-linear system dynamics of a moving vehicle can be modeled using INS measurements. The Pinson Error Modelmay be used to describe the state dynamics of $\boldsymbol{x}$. A 15 state Pinson INS Error Model can be described as the following [19]:

$$\boldsymbol{x} = \begin{bmatrix} \delta p_n \\ \delta p_e \\ \delta p_{down} \\ \delta v_n \\ \delta v_e \\ \delta v_d \\ \epsilon_n \\ \epsilon_e \\ \epsilon_d \\ b_{a_x} \\ b_{a_y} \\ b_{a_z} \\ b_{g_x} \\ b_{g_y} \\ b_{g_z} \end{bmatrix} \tag{17}$$

where,

$\delta p_n, \delta p_e, \delta p_{down}$ is NED position errors

$\delta v_n, \delta v_e, \delta v_d$ represents NED velocity errors

$\epsilon_n, \epsilon_e, \epsilon_d$ are the tilt errors about the NED axis

$b_{a_x}, b_{a_y}, b_{a_z}$ are accelerometer time-correlated biases

$b_{g_x}, b_{g_y}, b_{g_z}$ are gyro time-correlated biases

The Pinson error model states propagate according to the linear dynamics equation:

$$\dot{\boldsymbol{x}} = \boldsymbol{F}(\hat{x}, ins)\boldsymbol{x} + w \tag{18}$$

where,

$\boldsymbol{F}$ is the inertial error dynamics model linearized about $\hat{x}$

w is white Gaussian noise characterized by $N(0, Q)$

The linearized dynamics model can be expressed as:

$$\begin{bmatrix} \dot{\delta p} \\ \dot{\delta v} \\ \dot{\delta \epsilon} \\ \dot{b_a} \\ \dot{b_g} \end{bmatrix} = \begin{bmatrix} F_{pp} & F_{pv} & F_{p\epsilon} & 0_{3\times3} & 0_{3\times3} \\ F_{vp} & F_{vv} & F_{v\epsilon} & C_s^n & 0_{3\times3} \\ F_{\epsilon p} & F_{\epsilon v} & F_{\epsilon\epsilon} & 0_{3\times3} & -C_s^n \\ 0_{3\times3} & 0_{3\times3} & 0_{3\times3} & F_{aa} & 0_{3\times3} \\ 0_{3\times3} & 0_{3\times3} & 0_{3\times3} & 0_{3\times3} & F_{gg} \end{bmatrix} \begin{bmatrix} \delta p \\ \delta v \\ \delta \epsilon \\ b_a \\ b_g \end{bmatrix} \tag{19}$$

where,

C_s^n is the standard direction cosine matrix representing platform attitude.

2.5 Noise Models

2.5.1 First Order Gauss Markov Process

FOGM is a low-pass filter on white Gaussian noise.

$$\boldsymbol{X}(t_{k+1}) = \boldsymbol{\Phi}\boldsymbol{X}(t_k) + W(t_k) \tag{20}$$

where,

$\boldsymbol{\Phi}$ is equal to $e^{\boldsymbol{F}\Delta t}$

$\boldsymbol{F}$ the dynamics model matrix is equal to $-\frac{1}{\tau}$

$W(t_k)$ is white Gaussian noise with zero mean and unity variance

2.5.2 Brownian Motion Process

A Brownian motion process is the integral of white Gaussian noise. It is a special case of a FOGM process where the time constant τ is infinity.

$$X(t) = \int_0^t w \, dw \tag{21}$$

where,

$X(t)$ is the systems response

$w \sim \mathcal{N}(0, \boldsymbol{Q})$ is white noise with a variance of Q

2.6 NavToolKit Plug and Play Navigation Frame work

The aerial magnetic navigation filter will be implemented using NavToolKit. NavToolKit is a plug-and-play framework designed to create modular components for real-time navigation filters. Pluggable modules for alternative navigation systems, such as magnetic navigation, can be used with existing INS models and estimation filters. This plug-and-play framework allows sensor modules, measurement processors, algorithms, and estimation filters to be designed separately then plugged into the framework

III. Methodology

The objective of the research is to design a functional magnetic navigation module in NavToolKit and demonstrate a magnetic navigation system with actual post-processed F-16 data. Description of the magnetic navigation filter will be in Section 3.1. This work will reference the previous research on Online Calibration by Maj. Aaron Canciani [20]. Section 3.2 will detail the F-16 data used for the analytical analysis of this navigational filter. Section 3.3 details the magnetic anomaly maps referenced by the magnetic navigation filter. Lastly, Section 3.4 provides insight into some of the tuning done to the filter.

3.1 Navigation Filter

The filter is part of a NavToolKit plug-and-play navigation framework used to implement magnetic navigation systems. The magnetic navigation filter can obtain a real-time navigation solution with F-16 flight sensor data playback. A magnetic navigation measurement processor was developed in NavToolKit for the navigation filter previously. This measurement processor is leveraged by this research. The navigation filter consists of an augmented extended Kalman Filter (EKF) to aid in positioning the inertial navigation system (INS). Existing modules for an EKF and an INS are available in NavToolKit. The magnetic navigation filter used in this thesis is detailed in the following sections.

3.1.1 Filter states

The augmented EKF is a combination of Pinson error model states, a world-frame bias state, first-order Gause Markov state, and Tolles-Lawson coefficient states. The Pinson error model includes error states for position, velocity, and attitude and sensor

bias states for the IMU as described in eq. (30). The bias state estimates a constant scalar magnetic intensity bias inherent to the compensation process for the aircraft disturbance field and space weather effects. A First-order Gauss Markov (FOGM) state to estimate low-frequency variations in the scalar magnetic intensity from space weather effects and additional unmodelled errors [1] . The final state block, the Tolles-Lawson model, includes 18 states that track the values for the 18 compensation coefficients [20]. The states of the complete augmented magnetic navigation model may be given as:

$$\boldsymbol{x} = [\boldsymbol{\delta_p}, \boldsymbol{\delta_v}, \boldsymbol{\epsilon}, \boldsymbol{a}, \boldsymbol{g}, bias_{mag}, fogm_{mag}, \boldsymbol{t_L}]^{\top}_{35x1}, \tag{22}$$

where,

$\boldsymbol{\delta_p}$ is the INS latitude, longitude, and altitude errors,

$\boldsymbol{\delta_v}$ are the INS north/east/down velocity errors,

$\boldsymbol{\epsilon}$ are the 3 INS tilt errors,

$\boldsymbol{a}$ and $\boldsymbol{g}$ are the 3 accelerometer and 3 gyroscope biases,

$bias_{mag}$ is the constant scalar magnetic intensity bias (dc bias),

$fogm_{mag}$ estimate low-frequency variations in the scalar magnetic intensity from space weather effects and additional unmodelled errors,

and $\boldsymbol{t_L}$ are the 18 Tolles-Lawson Coefficients.

3.1.2 System Dynamics

There is no known prior dynamic coupling between the Pinson error model, the Tolles-Lawson model, the world-frame time-correlated bias, and the vector magne-

tometer states. The Pinson error model is given by $\boldsymbol{P}$ modeled using INS measurements and a linearized INS error model. This dynamics model is previously discussed in Section 2.4, and eq. (18). Note that the Tolles-Lawson states are modeled as Brownian motion and have constant dynamics and a linearly growing variance [20]. The $bias_{mag}$ is modeled as a constant DC bias. The $fogm_{mag}$ state is modeled as FOGM process with dynamics determined by a time constant τ [20].

$$\dot{x} = \boldsymbol{F}\boldsymbol{x} + w \tag{23}$$

describes the dynamics of the combined states where,

$$\boldsymbol{F} = \begin{bmatrix} \boldsymbol{P}_{15x15} & 0_{15x1} & 0_{15x1} & 0_{15x18} \\ 0_{1x15} & 0_{1x1} & 0_{1x1} & 0_{1x18} \\ 0_{1x15} & 0_{1x1} & -1/\tau & 0_{1x18} \\ 0_{18x15} & 0_{18x1} & 0_{18x1} & \boldsymbol{Tl}_{18x18} \end{bmatrix} \tag{24}$$

The term w is additive white Gaussian noise with zero-mean and a variance given by $Q = E[w^2]$. Q is given as

$$\boldsymbol{Q} = \begin{bmatrix} \boldsymbol{Q}_{P15x15} & 0_{15x1} & 0_{15x1} & 0_{15x18} \\ 0_{1x15} & 0_{1x1} & 0_{1x1} & 0_{1x18} \\ 0_{1x15} & 0_{1x1} & 2\sigma_{wf}/\tau_{wf} & 0_{1x18} \\ 0_{18x15} & 0_{18x1} & 0_{18x1} & \boldsymbol{Q}_{Tl18x18} \end{bmatrix}_{35x35} . \tag{25}$$

Q_P is the dynamics noise model for the inertial navigation system comprised of velocity random walk, angular random walk, an accelerometer, and gyroscope driving noise.

Q_{TL} is the noise model for the Tolles-Lawson coefficients, which are modeled as

Brownian motion. Parameter in achieving best performance for the navigation filter.

Tolles-Lawson coefficients modeled as Brownian noise mean the Tolles-Lawson coefficients have variances that grow linearly in time. Q_{TL} is composed of

$$Q_{TL} = \begin{bmatrix} Q_{perm3x3} & 0_{3x6} & 0_{3x9} \\ 0_{6x3} & Q_{ind6x6} & 0_{6x9} \\ 0_{9x3} & 0_{9x6} & Q_{eddy9x9} \end{bmatrix}_{18x18} . \tag{26}$$

$Q_{perm3x3}$ models the linear drift of the variance of hard-iron magnetic sources (permanent fields).

Q_{ind6x6} models the linear drift of the variance of soft-iron magnetic sources (induced fields).

$Q_{eddy9x9}$ models the linear drift of the variance of eddy-current magnetic sources.

3.1.3 Magnetic Navigation Measurement Module

A magnetic navigation measurement processor uses scalar intensity measurements to refine the state's estimates for position error. The measurement equation for the Tolles-Lawson augmented magnetic navigation filter is performing both map interpolation and Tolles-Lawson calibration.Consider the equation for scalar magnetic intensity measurements in a flight environment

$$z_t = B_{anomaly} + B_{core} + B_{dist} + B_{swe} + v \tag{27}$$

where,

$B_{anomaly}$ is the anomaly field value,

B_{core} is the Earth's core field value,

B_{dist} is the aircraft disturbance field value,

B_{swe} is the field contributed by space weather effects.

v additive white Gaussian noise (AWGN) v with variance σ^2_{mag}

The anomaly field is given by;

$$B_{anomaly} = f^{3D}_{map}(lat, long, alt) \tag{28}$$

where f^{3D}_{map} is an interpolation function over a magnetic anomaly map given INS corrected latitude, longitude, and altitude. The maps used with this filter are at altitudes 1066m, 2134m, and 5334m, see Section 3.3 for more details. The 3-D grid is created from a layered set of upward continuations of a 2-D magnetic anomaly map.

The Earth's Core field is computed by

$$B_{core} = W_{MM}(lat, lon, alt, time) \tag{29}$$

where W_{MM} is the World Magnetic Model (WMM), a function of INS latitude, longitude, altitude, and time. Note that magnetic anomaly maps have had the core field removed. However, the scalar measurement includes the core field. Using the World Magnetic Model (WMM) the core field can be added when estimating the measurement.

The aircraft disturbance field is estimated using the Tolles-Lawson compensation model as explained in Section 2.2.3, and it is given by

$$B_{dist} = C(\boldsymbol{A}, \boldsymbol{x}_{tl}) \tag{30}$$

$C(\boldsymbol{A}, \boldsymbol{x}_{TL})$ is a function of the direction cosine matrix $\boldsymbol{A}$, which uses vector magnetometer measurement (B_X, B_y, B_z) and the 18 Tolles-Lawson calibration coefficients $\boldsymbol{x}_{TL}$. The $\boldsymbol{A}$ matrix made up of direction cosines and their time derivatives. The directional cosines are formed by dividing each vector magnetometer axis by the scalar magnetometer measurement, rather than with the norm of the vector magnetometer flux-gate measurement.

The last component of the measurement equation is from space weather effects, given by:

$$B_{swe} = FOGM_{mag} \tag{31}$$

Implementation of the measurement equation into the navigation filter results in a non-linear measurement model. The general form for an Extended Kalman Filter measurement equation is given as:

$$z_t = h(x) + v \tag{32}$$

For the magnetic navigation filter, the measurement function $h(x)$ is given as:

$$h(x) = f_{map}^{3D}(lat_c, lon_c, alt_c) + W_{mm}(lat_c, lon_c, alt_c, t) + FOGM_{mag} + bias_{mag} + C(\boldsymbol{A}, \boldsymbol{x}_{tl}), \tag{33}$$

with

f_{map}^{3D} as a interpolation function over a magnetic anomaly map,

W_{MM} as the World Magnetic Model interpolation function to obtain the core field intensity,

$FOGM_{mag}$ First-Order Gauss Markov Process, and

$bias_{mag}$ dc bias.

$C(\boldsymbol{A}, \boldsymbol{x}_{tl})$ is the function which computes the Tolles-Lawson compensation and estimate the aircraft disturbance field, and

v is white Gaussian Noise

The measurement Jacobian is most complex part of the Tolles-Lawson augmented MagNav EKF. The measurement Jacobian created through a mix of both finite differencing and analytical Jacobians. The measurement equation only interacts with a subset of the 38 states in the overall measurement filter [1]. The measurement Jacobian is:

$$\boldsymbol{H} = \left[\frac{\delta_z}{\delta \delta lat}, \quad \frac{\delta_z}{\delta \delta lon}, \quad 0_{1x13}, \quad 1, \quad 1, \quad \boldsymbol{A}_{1x18} \right], \tag{34}$$

where

$\frac{\delta_z}{\delta \delta lat}, \frac{\delta_z}{\delta \delta lon}$ two terms in the Jacobian represent the gradient of the magnetic field maps (anomaly field plus core field).

$\boldsymbol{A}$ is the Tolles-Lawson Jacobian matrix and is easily read off directly from the measurement equation Tolles-Lawson function $C(\boldsymbol{A}, \boldsymbol{tl})$ given in Equation (33).

The contribution of the $bias_{mag}$, and $FOGM_{mag}$ results in the 1's

3.2 F-16 data

Data used in this thesis was recorded on a F-16 platform. The U.S. Air Force Test Pilot School (TPS) collected magnetic navigation flight test data during September 2020 [21]. The test data consisted of 17 flight tests that were flown on an F-16 carrying RASCAL Pod. All flight were flown over Edwards Air Force Base, CA see Figure 9 for overview of flight profiles. The following component data is used:

1. Scalar Magnetic Intensity Measurements: Collected at 1kHz from a Geometrics MFAM Scalar Magnetometer

2. Vector Magnetic Field Measurements: Collected at 1kHz from a Geometrics MFAM Vector Magnetometer

3. Truth Position, Velocity, and Attitude: GPS-aided INS output of aircraft whole state. Provided by Time and Space Positioning Information system (TSPI)).

4. IMU data: Colllected at 10 Hz from a High-performance tactical-grade Honeywell HG1700

The scalar and vector magnetometer data is filtered using a Butterworth low-pass filter. TSPI data is used for the truth PVA and Altitude. The scalar, vector, and altitude data are down-sampled to 10 Hz for ease of computing.

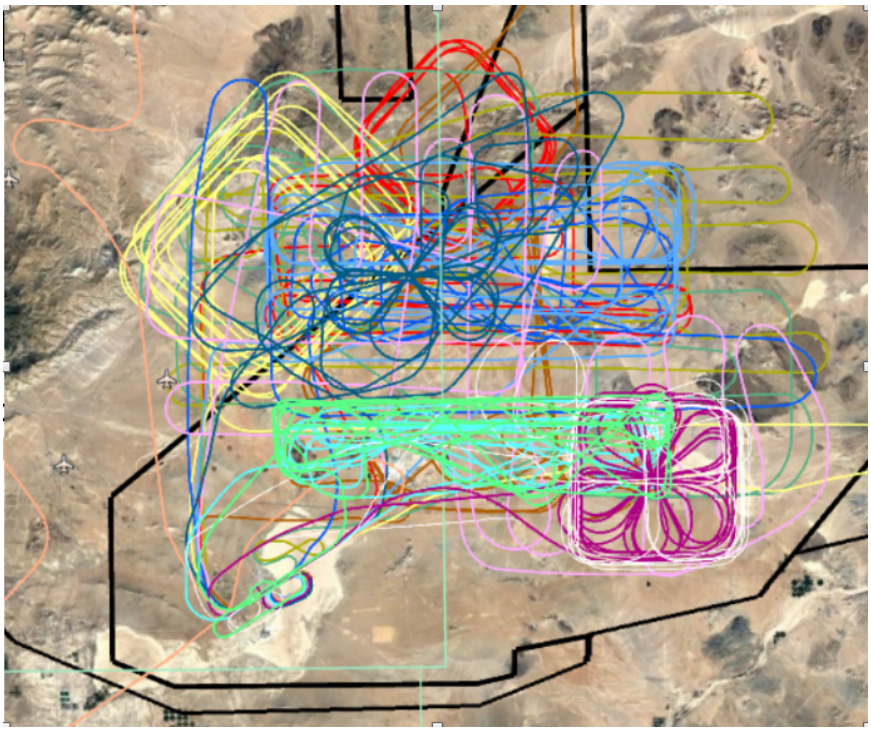

Figure 9: 17 Flight Profiles[21]

3.2.0.1 Flight Profiles

A majority of testing was flown over high fidelity anomaly maps, as detailed in Section 3.3. Out of 17 test flights that were executed, eight profiles were selected for this research and are summarized in Table 1. Each flight profile is approximately 60 minutes within the magnetic anomaly map area. The portions of the flight that are not within the mapped area are removed.

The flight profiles consisted of five maneuvers: low-altitude, medium-altitude, 3D, rectangular calibration, and cloverleaf calibration. The low altitude maneuvers consisted of constant altitude, constant heading (1D profiles), 1-3g turns (2D profiles) flown over the map at altitude (1066 m). Test points consisted of 60 minutes of free play during which the pilot maintained altitude ±50ft within the lateral confines of the anomaly map boundaries. The intent was to cover as much of the map area as possible using 2-3g turns unless faster dynamics were needed for safety of flight [21].Medium altitude maneuvers consisted of constant-altitude 1-3g turns (2D profiles) flown over the medium altitude map (7,000 ft MSL). Test points consisted of 60 minutes of free play during which the pilot maintained altitude and airspace within the specified map

Table 1: Summary of F-16 flight profiles

Profile	**Altitude, MSL (m)**	**Date**	**Maneuvering**	**Acft. Magnetic Env.**
1	1066	10 Sept 20	Low-Altitude	Quiet
2	2134	10 Sept 20	Med-Altitude	Quiet/Loud
3	2134	15 Sept 20	Med-Altitude	Loud
4	2134-5334	11 Sept 20	3D	Quiet
5	2134-5334	16 Sept 20	3D	Quiet/Loud
6	2134-5334	21 Sept 20	3D	Quiet/Loud
7	9144-2438	17 Sept 20	Cal-Rectangle Med-Altitude	Quiet/Loud
8	9144-2438	18 Sept 20	Cal-Clove Med-Altitude	Quiet

boundaries [21]. 3D maneuvers were flown using 2-3g turns and vertical maneuvers at ±10 degrees of pitch (3D flight profiles) flown between the medium altitude and cap altitude maps (2134 - 5334 m). Similar to the low and medium altitude maneuvers, 3D maneuver test points consisted of approximately 60 minutes of flight on conditions [21]. For the calibration maneuvers on each of the straight sections (4 total) of the patterns (inner straight sections on the cloverleaf pattern), a series of yaw, roll, and pitch maneuvers were executed[21].Two categories for aircraft magnetic environment configuration were established for flight test: quiet and loud. The only difference between quiet and loud was the use of the radar during the loud configuration.

3.3 Magnetic Anomaly Maps

Three high fidelity magnetic maps are used for the magnetic navigation filter. The three magnetic anomaly maps were created by Sander Geophysics Limited over Edwards Air Force Base, California in 2019 [22]. Map details are summarized in Table 2. The maps are shown in Figure 10 , 11, and 12.

Table 2: Summary of Edwards Air Force Base magnetic anomaly maps.

Map Name	**Map Altitude (m)**	**Traverse line Spacing (m)**	**Control Line Spacing (m)**
Cords Road	1066	300	3000
Medium Altitude	2134	1200	6000
Cap Altitude	5334	4800	12000

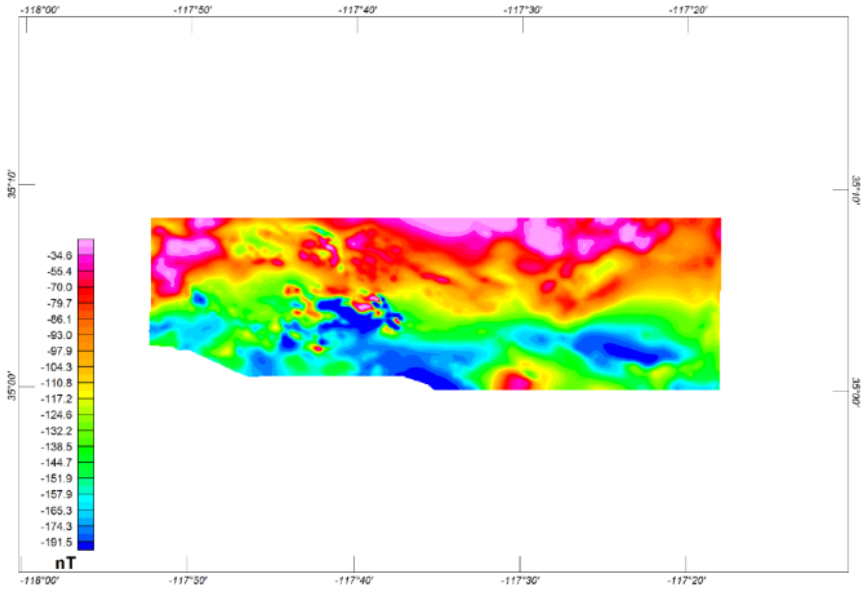

Figure 10: Cords Road anomaly map (1066 m) [22]

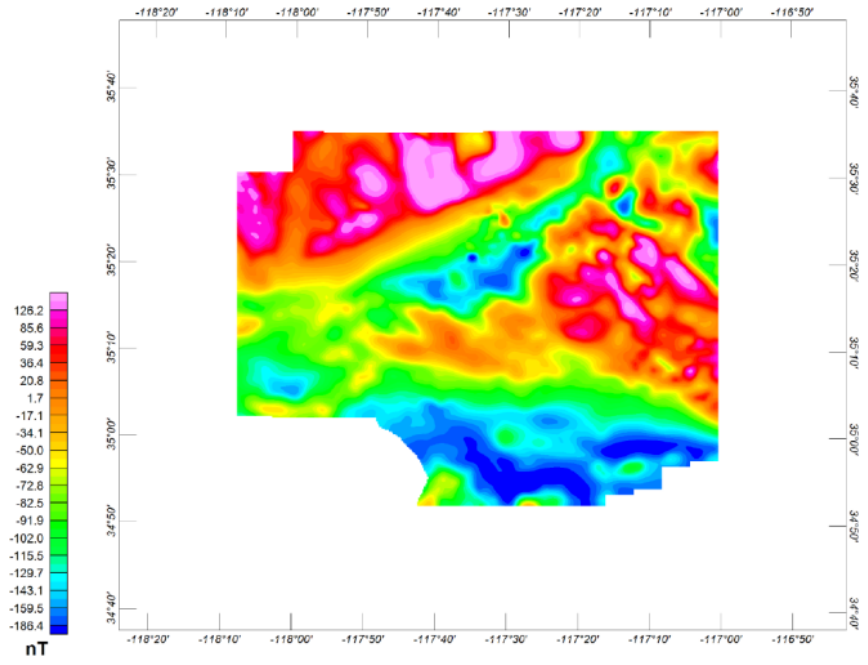

Figure 11: Medium altitude anomaly map (2134 m)[22]

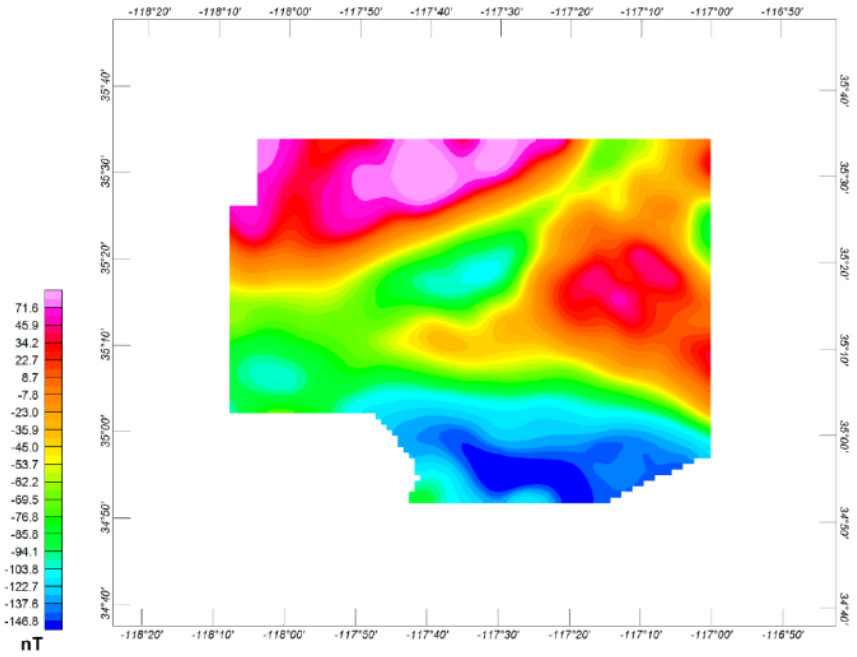

Figure 12: Cap altitude anomaly map (5334 m) [22]

3.4 Filter Tuning

3.4.1 FOGM State

The standard deviation and time constant of the FOGM state are tuned so that it can estimate the space weather effects and other modeling errors in the navigation solution. For each F-16 flight profile, the FOGM model parameters are estimated by observing the static Tolles-Lawson compensation error. The σ_{Fogm} is estimated by simply taking the standard deviation of the compensation error, which is the unbiased measured aircraft disturbance minus the unbiased estimated aircraft disturbance. Observing the compensation error's auto-correlation, τ_{Fogm} is when the compensation error decreases to 36.8% of its starting value. The time constant describes how quickly the data decorrelates with itself. The Python functions from the Scipy Signal Library, Correlate, and Correlate Lags are used to compute the auto-correlation of the compensation error, see table 3 for each profile tuning parameters. See fig. 13, for example, using Profile 1.

Table 3: Magnetic Anomaly Navigation Filter Tuning Parameters

Profile Name	**Smag Cov**	**Vmag Cov**	$Fogm_{Mag}$ σ_{FOGM}	$Fogm_{mag}$ τ_{FOGM}	$bias_{mag}$ σ_{bias}
1	116	[50,50,50]	10	30	1000
2	116	[50,50,50]	10	32	1000
3	116	[50,50,50]	17	11	1000
4	116	[50,50,50]	33	384	1000
5	116	[50,50,50]	23	45	1000
6	116	[50,50,50]	21	146	1000
7	116	[50,50,50]	70	150	1000
8	116	[50,50,50]	72	881	1000

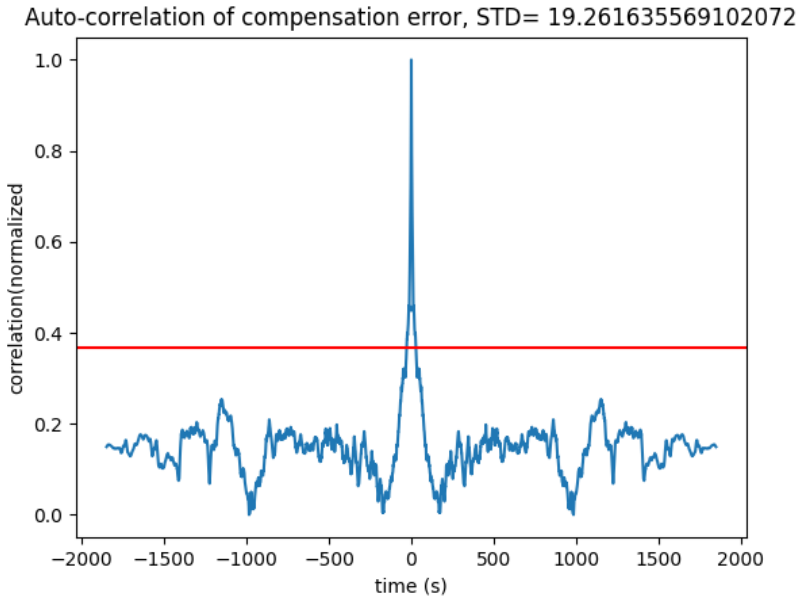

Figure 13: Profile 4 auto-correlation with a line at 36.8%

3.4.2 Tolles-Lawson Coefficient State Covariance

Tolles-Lawson coefficients can be determined by the linear model of form $y = Ax$. The $\boldsymbol{A}$ matrix can determine the estimate of the uncertainty of the coefficients. Also, the $\boldsymbol{A}$ matrix can also help calculate the model fit error $e = y - \boldsymbol{A}\boldsymbol{x}_{TL}$. The initial covariance of the Tl state can be formed by:

$$\boldsymbol{P}_{TL} = (\boldsymbol{A}^\top \boldsymbol{A})^{-1} var(e), \tag{35}$$

$\boldsymbol{P}_{TL}$ allows the EKF to start with information of the cross-correlations between the Tolles-Lawson coefficients

IV. Results and Analysis

This chapter presents the results and analysis of online calibration compared to static calibration. Three scenarios are analyzed in the performance of online calibration. Section 4.1, static and online calibrations are performed on all eight profiles and analyzed using each profiles data. Section 4.3, static and online calibration performance is analyzed using profile 1's data for calibration for each profile. Profile 1 is utilized because it is one of the earlier flights flown out of the profile set. Section 4.2 is similar to the second scenario with added GPS measurement. The GPS aided results are then analyzed. All this will be compared to the navigation filter's performance if no GPS or alternative navigation aid is available. The inertial navigation system (INS) drift see table 4 for each profile INS drift. The analysis of these methods gives us a suitable basis for the performance of the online calibration.The measurement used to compare the calibration performance is the distance roots mean square (DRMS) of the position error.

4.1 Online Calibration

Static and online calibration is used in the navigation filter for every flight profile. This scenario uses the first half of each profile to perform a static calibration, obtaining the calibration coefficients. When using online calibration with the navigation filter, the calibration coefficients are then used to initialize the Tolles-Lawson coefficient state. This differs from the static calibration case where the coefficient remains static in the navigation filter. The navigation filter using static coefficients is used to compare the performance of the online calibration. This comparison shows how well the online calibration performed under the exact condition of the filter using static calibration coefficients. See table 4 for each profile's static and online calibration

Table 4: Position Error $DRMS(m)$ results for each flight profile using Static and Online calibrations

Profile Name	**Unaided INS** $DRMS(m)$	**Static Cal.** $DRMS(m)$	**Online Cal.** $DRMS(m)$	**Online - Static Cal.** $DRMS(m)$
1	2328	152	134	-18
2	4444	557	578	21
3	2412	373	371	-2
4	2566	1091	949	-142
5	2933	490	485	-5
6	3010	327	314	-13
7	1211	1264	1124	-140
8	4570	1121	1109	-12
Average	3035.12	624.025	609.5	-15.125

performance results.

For the navigation filter using static coefficients, the first 30-minutes of flight data is used to calibrate each profile, obtaining the calibration coefficient. Then the entire 60 min flight data is processed in the navigation filter. The same procedure is used for all flight profiles. Similarly, the same is done for the filter using online calibration. However, the static calibration performed in the first 30 minutes obtains the coefficients used to initialize the Tolles-Lawson coefficient state coefficients. The significant difference in the static and online calibration is the state of the coefficients. In the navigation filter using static calibration, the coefficients stay static for the flights entirely; however, in the navigation filter using online calibration, the coefficients are adjusted as the filter is updated.

The performance of online calibration is improved over that of static calibration. Profiles 4 and 7 online did better than the other profiles, they achieved 140m of error DRMS less than the static calibration. Online calibration in this scenario shows to be a suitable method with similar or improved performance to the static calibration method. Figure 14 shows the position error results and the DRMS achieved by both

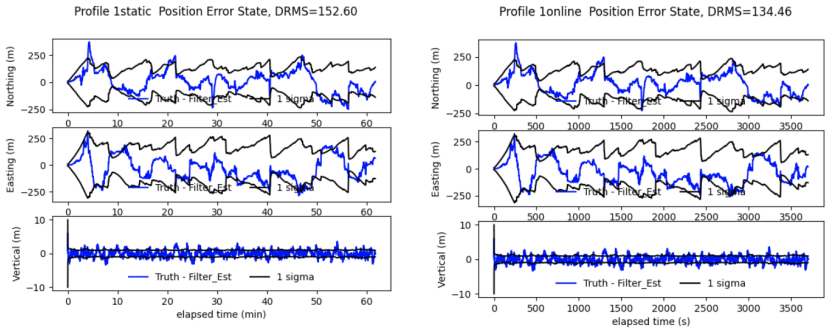

Figure 14: Comparing profile 1 with scenario 1 using static(left) and online(right) methods.

methods. The performance by the filter using static and online calibration have very similar results; however, online calibration improves by 18m DRMS. Profile 1 is one of the first flights flown by calendar date and will be used in the following scenarios.Also, Figure 15 shows the online calibration navigation filter updates and changes to the first three coefficients in the Tolles-Lawson coefficients state, confirming that the coefficients are not remaining static.

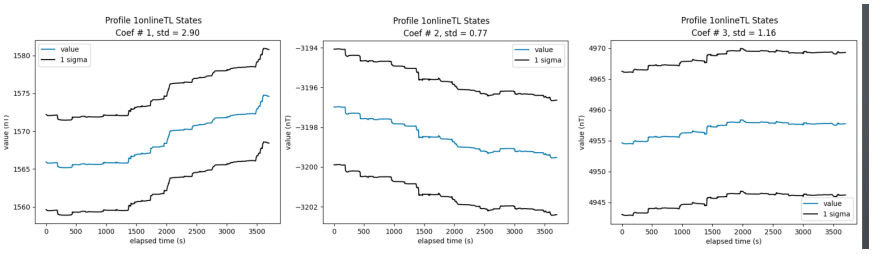

Figure 15: Profile 1's first three coefficients in scenario 1 using online calibration.

4.2 Online with different flight Coefficients

During this test, the static calibration coefficients are set using profile 1, and these calibration coefficients are used for all remaining flights. Both filters using static and online calibration use previous days' calibration coefficients. Operationally this is not ideal because of the many different factors that could change the calibration, like the aircraft's configuration. Updating the coefficients in the navigation filter using online calibration is more beneficial for aircraft operations as it reduces the need to update the aircraft's calibration. Table 5 provides the results for this test.

Online calibration achieved better results for all the profiles when initializing with coefficients from profile 1. The position error DRMS of each profile increased because calibration coefficients were incorrect. This increase was expected. However, the online calibration method's position error was less than the static calibration method for all profiles. The results suggest that the online calibration method has a more suitable performance by updating the calibration coefficients. The profile that had the best performance over static calibration is flight profile 8, where the online calibration method achieved a better result by 302m. Profile 8 is split into two different

Table 5: Static and Online Calibration using Profile 1 static coefficients

Profile Name	**Profile Altitude**	**Unaided INS**	**Static Cal.**	**Online Cal.**	**Online - Static**
	(m)	$DRMS(m)$	$DRMS(m)$	$DRMS(m)$	$DRMS(m)$
1	1066	2328	152	142	-10
2	2134	4444	477	454	-23
3	2134	2412	1145	875	-270
4	2134-5334	2566	1430	1272	-158
5	2134-5334	2933	735	708	-27
6	2134-5334	3010	589	495	-94
7	9144-2438	1211	2530	2369	-161
8	9144-2438	4570	2450	2148	-302
Average		3035.12	1188.5	1057.875	-130.625

altitudes of 9144m for the first half and 2438m in the second, see Figure 16. . Important to note that the calibration coefficients used to initialize the online calibration method Tolles-lawson state were accomplished at 1066m of altitude. Since the static calibration coefficients remain static for the entirety of the flight, the compensation increases in error, causing the increase of position error. Due to the update of the coefficients, the online filter estimate is more accurate, causing the filter to achieve better results. The error between the scalar magnetometer measurement and the filter's estimated measurement can be seen in the online case in Figure 17. The standard deviation of the measurement and the estimated measurement using the online calibration method is 139.05. Using the static calibration method, it is 139.14. The difference in the standard deviation suggests that the online calibration method estimate reflects the scalar magnetometer measurement. With the difference in the altitude from profile 1 and the altitude of profile 8, the static calibration method cannot correctly estimate the measurement using the calibration coefficients obtained from

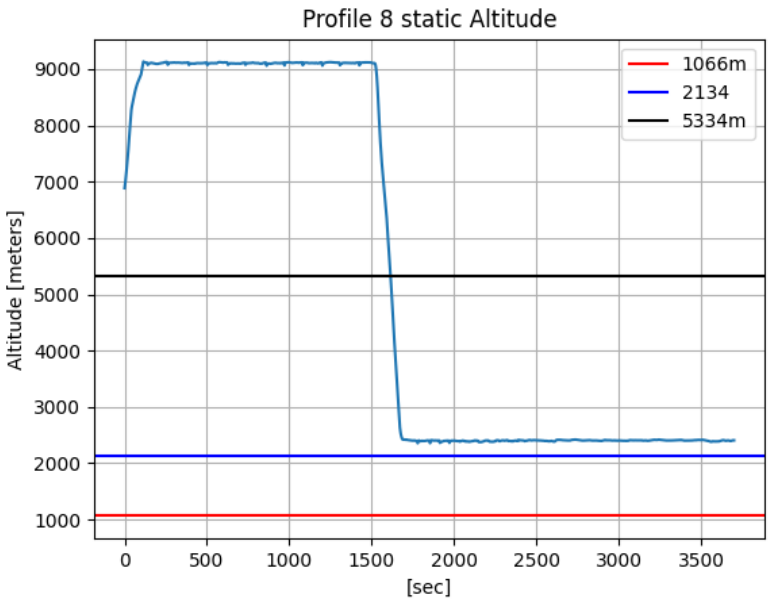

Figure 16: Altitude Profile (Profile 8)

profile 1. However, the online calibration method results suggest that adjusting the calibration coefficients better reflect the magnetometer measurement at the altitude flown in profile 8. Section 4.3 includes how static calibration results differ at different altitudes.

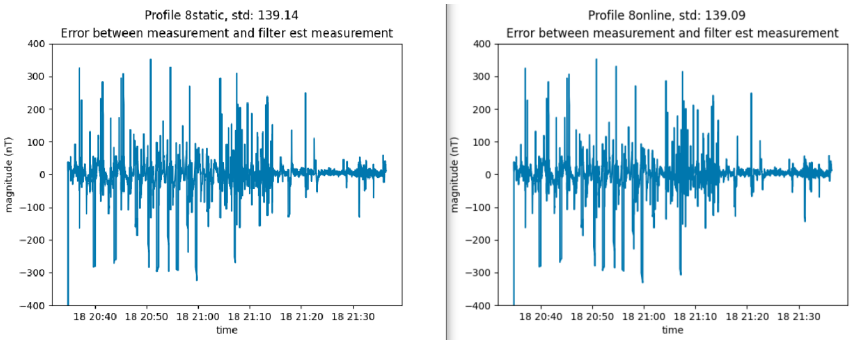

Figure 17: Unbiased error between measurement and filter estimate for both static method (left) and online method (right) for Profile 8

4.3 Online with different flight Coefficients and GPS Aid

This scenario uses the same setup as Section 4.2 using online calibration with set coefficients from profile 1. However, this scenario includes GPS measurements at the beginning of the flight for two cases: 5 and 10 minutes. The flight analysis shows that the filter could better adjust the calibration coefficients during altitude changes with online calibration. As expected, the position error decreases with the GPS aid as the filter adjusts the coefficients. Table 6 provides the results for this test.

There is significant improvement with profile 7,8 when using GPS measurement to aid the navigation solution. Profiles 7,8 have two common factors, a significant difference in altitude from the profile used for calibration and significant altitude change during the flight. Due to this change of flight altitude with online calibration, the filter adjusted the coefficients to compensate for the aircraft disturbance field. In section 4.2, there is some improvement with online calibration without any aid of GPS. As we expected, the navigation filter improved significantly with online calibration with the short amount of GPS aid. The GPS aid allows the filter to adjust the coefficients to reasonably reflect the aircraft disturbance field during the flight Figure 18

Table 6: GPS Aid To Online Calibration Using Profile 1 static coefficients

Profile Name	**Profile Altitude** (m)	**No GPS** $DRMS(m)$	**5 Min GPS** $DRMS(m)$	**10 Min GPS** $DRMS(m)$
1	1066	142	132	154
2	2134	454	384	513
3	2134	875	811	791
4	2134-5334	1272	749	979
5	2134-5334	708	665	575
6	2134-5334	495	489	572
7	9144-2438	2369	482	427
8	9144-2438	2148	650	204
Average		1057.87	545.25	526.875

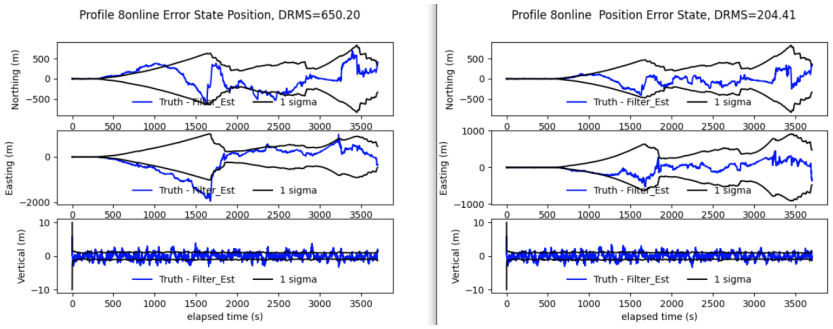

Figure 18: Profile 8 Position Error with 5 min(left) and 10 min (right) of GPS Aid

shows the position state error and covariance bounds for profile 8 with GPS aid. This adjustment is a benefit over static calibration due to the different altitudes. Figure 16 shows the flight altitudes for profile 8.

The results of the static calibration method using profile 1's coefficient on profile 8's navigation filter show that static calibration does not perform satisfactorily. The static calibration method cannot use the static calibration coefficients to estimate the aircraft disturbance field as accurately as the online method. The lack of accuracy is shown by comparing the static calibration of the entire flight to the static calibration of the flight broken up into the two sections counting the different altitudes see Figure 16 for profile altitudes. Figure 19 shows the error between the measured aircraft field and the estimated aircraft field using static calibration for the entire duration of the flight. This figure shows the error magnitude of the ranges between 300 to -200nt and the error standard deviation of 89.78 containing the altitude difference of 9144m to 2438m. The entire flight is then compared to Figure 20, which shows the error between the measured aircraft field and the estimated aircraft field using static calibration for the first flight section containing the first altitude of 9144m. The magnitude of the error lessens to $\pm 100nt$ and a error standard deviation of 74.80. The entire flight is also compared to Figure 21 which shows the error between the measured aircraft field and the estimated aircraft field using static calibration for the

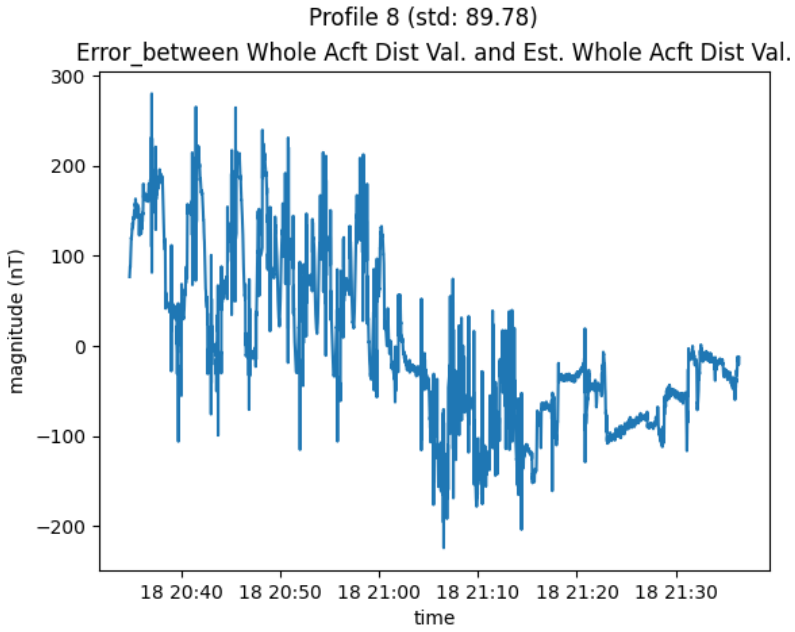

Figure 19: Entire profile error between aircraft disturbance measurement and estimated aircraft disturbance for Profile 8

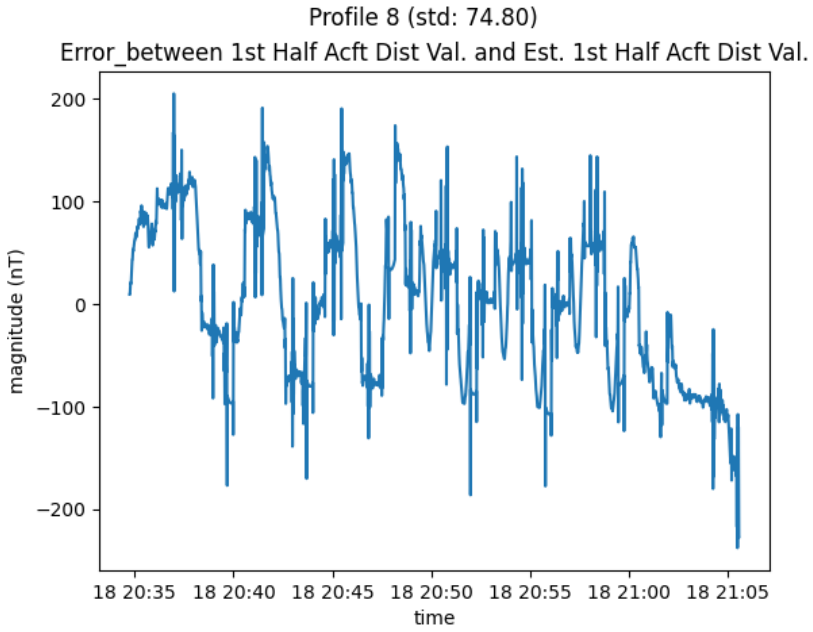

Figure 20: First half error between aircraft disturbance measurement and estimated aircraft disturbance for Profile 8

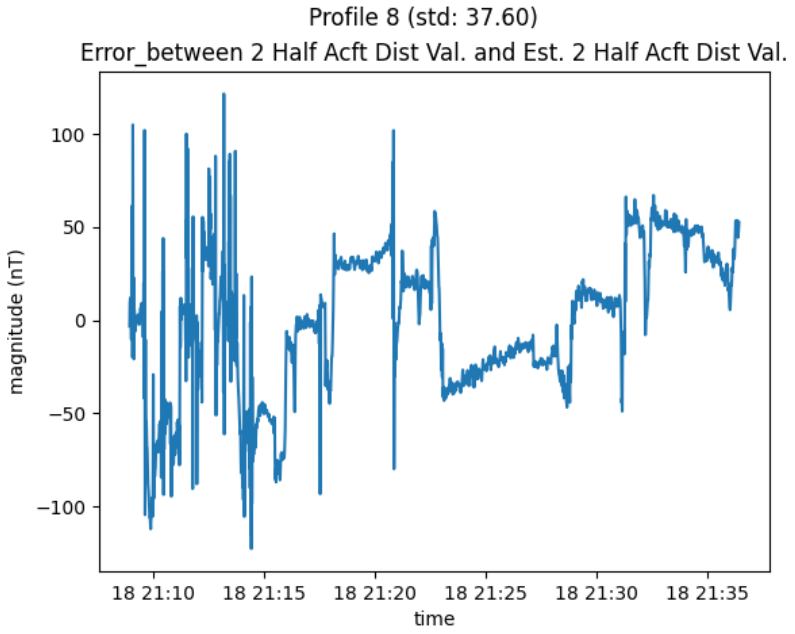

Figure 21: Second First half error between aircraft disturbance measurement and estimated aircraft disturbance for Profile 8

second section of the flight containing the second altitude of 2438m. The magnitude of the error lessens to $\pm 100nt$, and the error standard deviation of 37.60. This suggests that calibration needs to be performed at each altitude for a more accurate estimate. Online calibration can adjust the calibration coefficients for a better estimate as flight altitudes change.

Adjusting the coefficients can better estimate the aircraft disturbance when flying at different altitudes. This adjustment may be necessary due to the changes in temperature as the aircraft changes altitude. These temperatures could affect the magnetic field of the components of the aircraft. As permanent material is heated, the magnetic field is reduced. However, when the temperature is decreased, the magnetic increases [23]. Suggesting that as the aircraft increases in altitude, the temperature decreases, increasing the aircraft's disturbance field. This would reflect why the static calibration cannot accurately estimate the aircraft disturbance field with static coefficients. However, the online calibration filter may account for the change of altitude

better predicting the disturbance field.

V. Conclusions

This chapter presents the conclusions and findings from this research and discusses future work to improve online calibration for magnetic anomaly navigation. This research sought to implement online navigation as a "plug and play" module and to analyze the performance of the online calibration across multiple F16 flight profiles.

Based on the results from simulation cases, a real-time magnetic navigation system can bound inertial navigation system (INS) drift and produce a navigation solution without the presence of a Global Positioning System (GPS). The online calibration can bound INS drift, update calibration coefficients and provide a navigation solution. This navigational filter showed that online calibration could perform better than static calibration. However, the items identified below in the future work section should significantly improve the overall filter performance and the accuracy of using online calibration.

5.1 Future Work

Results obtained in this thesis show promise for magnetic anomaly navigation. Further work needs to be accomplished to obtain a working NavToolKit plug and play module to perform online navigation calibration. There are three things identified during this research that can further enhance the performance of the online magnetic navigation filter.

5.1.1 Tolles Lawson Regression Compensation

First, a better regression compensation method algorithm. The current algorithm uses Tolles Lawson's least squares regression repeated multiple times to fit the data and get the calibration coefficients.

5.1.2 Measurement Proscessor Direction Cosines

Second, the NavToolKit measurement processor is currently buffering the vector measurements, and calculating the gradient of these vectors. Then to calculate the direction cosines and differential directional cosines, it divides the vector by the scalar and the gradient by the scalar. However, this does not give us all the information we need for the calibration. Ideally, the filter would bring a scalar and vector measurement simultaneously. It would then calculate the directional cosines by dividing the vector by the scalar, for the differential directional cosines calculating them by using the directional cosines. Adjusting the measurement processor algorithm should allow for better performance of the navigation filter.

5.1.3 Including Schimdt States

Third, Extend Kalman Filter Schmidt states require implementation into NavToolKit modules to reflect the research done by Aaron Canciani on online calibration. The Schmidt states are sometimes referred to as consider states because they are considered but not implemented literally in the filter []. This state module will include the vectors states used in this Online Calibration Paper.

Bibliography

1. Aaron Canciani and John Raquet. Absolute Positioning Using the Earth's Magnetic Anomaly Field. *Navigation, Journal of the Institute of Navigation*, 63(2):111–126, 2016.

2. Fausto Fiorillo. Magnetic Field Sources. In *Characterization and Measurement of Magnetic Materials*, pages 105–157. Elsevier, 2004.

3. Arnaud Chilliat, Susan Macmillan, Patrick Alken, Ciaran Beggan, Manoj Nair, Brian Hamilton, Adam Woods, Victoria Ridley, Stefan Maus, and Alan Thomson. The US / UK World Magnetic for 2015-2020. *NOAA National Geophysical Data Center*, pages 1–112, 2015.

4. Daniel J. Clarke. Real-time Aerial Magnetic and Vision-aided Navigation. Master's thesis, AFIT, 2021.

5. N. Olsen G. Hulot, A. Balogh, U.R. Christensen, C. Constable, M. Mandea, editor. *Terrestrial Magnetism*. Springer New York, 1 edition, 2011.

6. Measuring Earth's Magnetism.

7. J.KORHONEN ET AL. World Digital Magnetic Anomaly Map NOAA candidate. *Helmholtz Centre Potsdam*, page 210.

8. Terence J. Sabaka, Nils Olsen, and Robert A. Langel. A comprehensive model of the quiet-time, near-Earth magnetic field: Phase 3. *Geophysical Journal International*, 151(1):32–68, 2002.

9. C. T. Russell. A Brief History Of Solar-Terrestrial Physics. In *Introduction to Space Physics*. 2019.

10. Colin. Reeves. Aeromagnetic Surveys: Principles, Practice and Interpretation. *Geosoft*, page 155, 2005.

11. Tail-mounted stinger on a geo-survey aircraft. http://sgl.com/MagTF.html. Accessed: 2021-08-06.

12. Luzhao Chen, Peilin Wu, Wanhua Zhu, Yongqiang Feng, and Guangyou Fang. A novel strategy for improving the aeromagnetic compensation performance of helicopters. *Sensors (Switzerland)*, 18(6), 2018.

13. Mitchell Hezel. Improving Aeromagnetic Calibration Using Artificial Neural Networks. Master's thesis, AFIT, 2020.

14. Walter E. Tolles and J.D. Lawson. *Magnetic Compensation of MAD Equipped Aircraft*. Mineola, NY, 1950.

15. Paul Leliak. Identification and Evaluation of Magnetic-Field Sources of Magnetic Airborne Detector Equipped Aircraft. *IRE Transactions on Aerospace and Navigational Electronics*, ANE-8(3):95–105, 1961.

16. Mandea Mioara and Monika Korte. Geomagnetic Observations and Models. *Springer Science and Business Media*, 2010.

17. P. S. Maybeck and George M. Siouris. Stochastic Models, Estimation, and Control, Volume I, 1980.

18. Brown Robert Grover and Patrick Y. C. Hwang. *Introduction to random signals and applied kalman filtering (second edition)*, volume 2. 1992.

19. David Titterton and John Weston. *Strapdown Inertial Navigation Technology*. 2004.

20. Aaron Canciani. Magnetic Navigation on an F-16 Aircraft using Online Calibration. *IEEE Transactions on Aerospace and Electronic Systems*, pages 1–15, 2021.

21. Daniel Clarke, Justin Soeder, Raina Duncan, Christopher Ames, Casey Horgan, and Bryce. Turner. A Limited Evaluation of Magnetic Anomaly Navigation, Project HAVE MANTA RAY. Technical report, U.S. Air Force Test Pilot School, Edwards AFB, CA, 2020.

22. Martin Bates and Aamna Sirohey. Aeromagnetic Navigation for United States Air Force Institute of Technology. Technical report, Sander Geophysics Limited, ON Canada, 2019.

23. Silvio Decurtins. Magnetic materials. fundamentals and device applications. edited by nicola spaldin. *Angewandte Chemie International Edition*, 42, 2003.

Acronyms

DGC Defence Geographic Centre. 5

DOD Department of Defence. 1, 2

EKF extended Kalman Filter. 4, 26

GPS Global Positioning System. 1, 51

INS inertial navigation system. 4, 22, 26, 40, 51

NGA National Geospatial-Intelligence Agency. 5

swp size, weight, and power. 10

TPS U.S. Air Force Test Pilot School. 32

TSPI Time and Space Positioning Information system. 33

WMM World Magnetic Model. 4, 30

REPORT DOCUMENTATION PAGE

Form Approved
OMB No. 0704–0188

1. REPORT DATE *(DD–MM–YYYY)*	2. REPORT TYPE	3. DATES COVERED *(From — To)*
07–03–2022	Master's Thesis	Sept 2018 — Mar 2020

4. TITLE AND SUBTITLE

Magnetic Navigation Using Online Calibration Filter Analysis

5a. CONTRACT NUMBER

5b. GRANT NUMBER

5c. PROGRAM ELEMENT NUMBER

6. AUTHOR(S)

Jonnathan D. Bonifaz Montesdeoca

5d. PROJECT NUMBER

5e. TASK NUMBER

5f. WORK UNIT NUMBER

7. PERFORMING ORGANIZATION NAME(S) AND ADDRESS(ES)

Air Force Institute of Technology
Graduate School of Engineering and Management (AFIT/EN)
2950 Hobson Way
WPAFB OH 45433-7765

8. PERFORMING ORGANIZATION REPORT NUMBER

AFIT-ENG-MS-22-M-010

9. SPONSORING / MONITORING AGENCY NAME(S) AND ADDRESS(ES)

Intentionally Left Blank

10. SPONSOR/MONITOR'S ACRONYM(S)

11. SPONSOR/MONITOR'S REPORT NUMBER(S)

12. DISTRIBUTION / AVAILABILITY STATEMENT

DISTRIBUTION STATEMENT A:
APPROVED FOR PUBLIC RELEASE; DISTRIBUTION UNLIMITED.

13. SUPPLEMENTARY NOTES

14. ABSTRACT

Magnetic navigation using the Earth's magnetic anomaly field has proven to be a promising alternative that can provide coverage for a navigation system. This research demonstrates a magnetic navigation system using an extended Kalman filter (EKF) to aid an aircraft's inertial navigation system (INS). Traditional magnetic anomaly navigation uses a "static calibration method," which takes post-processed data to calibrate, obtaining the Tolles-Lawson coefficients needed for magnetic anomaly navigation filter compensation. These coefficients are constant and may cause drifts in the navigation filter if not re-calibrated. The online calibration method continuously updates the Tolles-Lawson coefficients as a filter state, reducing the need for calibration flights. This research uses F-16 data to demonstrate the effectiveness of this method.

15. SUBJECT TERMS

Magnetic Navigation, Extended Kalman filter, Inertial Navigation, Magnetic Navigation Calibration

16. SECURITY CLASSIFICATION OF:			17. LIMITATION OF ABSTRACT	18. NUMBER OF PAGES	19a. NAME OF RESPONSIBLE PERSON
a. REPORT	b. ABSTRACT	c. THIS PAGE			Maj. Joseph A Curro, AFIT/ENG
U	U	U	UU	67	19b. TELEPHONE NUMBER *(include area code)* (937) 255-3636, ext 4620; joseph.curro@afit.edu